Biochimica et Biophysica Acta 1828 (2013) 1982–1988

Contents lists available at SciVerse ScienceDirect

Biochimica et Biophysica Acta

journal homepage: www.elsevier.com/locate/bbamem

Insertion of TAT peptide and perturbation of negatively charged model phospholipid bilayer revealed by neutron diffraction

Xiaochao Chen [a,b], Farid Sa'adedin [b], Bruno Deme [c], Pingfan Rao [a], Jeremy Bradshaw [b,*]

[a] Institute of Biotechnology, Fuzhou University, 4th Floor, Qing-gong Building, No.523, Gongye Road 350002, Fuzhou, Fujian, People's Republic of China
[b] The University of Edinburgh, Royal (Dick) School of Veterinary Studies, Easter Bush, Roslin, Midlothian EH25 9RG, UK
[c] Institut Laue-Langevin, 6 rue Jules Horowitz, BP 156, F-38042 Grenoble Cedex 9, France

ARTICLE INFO

Article history:
Received 18 January 2013
Received in revised form 22 April 2013
Accepted 23 April 2013
Available online 1 May 2013

Keywords:
Cell penetrating peptide
TAT peptide
Neutron diffraction
Phospholipid

ABSTRACT

TAT peptide is one of the best-characterized cell penetrating peptides derived from the transactivator of transcription protein from the human immunodeficiency virus 1. The aim of this study was to investigate the interaction between TAT peptide and partially negatively-charged phospholipid bilayer by using lamellar neutron diffraction. The main findings are the existence of a contiguous water channel across the bilayer in the presence of TAT peptide. Taken in combination with other observations, including thinning of the lipid bilayer, this unambiguously locates the peptide within the lipid bilayer. The interaction of TAT peptide with anionic lipid bilayer, composed of an 80:20 mixture of DOPC and DOPS, takes place at two locations. One is in the peripheral aqueous phase between adjacent bilayers and the second is below the glycerol backbone region of bilayer. A membrane thinning above a peptide concentration threshold (1 mol%) was found, as was a contiguous transbilayer water channel at the highest peptide concentration (10 mol%). This evidence leads to the suggestion that the toroidal pore model might be involved in the transmembrane of TAT peptide. We interpret the surface peptide distribution in the peripheral aqueous phase to be a massive exclusion of TAT peptide from its intrinsic location below the glycerol backbone region of the bilayer, due to the electrostatic attraction between the negatively-charged headgroups of phospholipids and the positively charged TAT peptides. Finally, we propose that the role that negatively-charged headgroups of DOPS lipids play in the transmembrane of TAT peptide is less important than previously thought.

1. Introduction

Over the past decades, the low permeability of cell membranes and poor targeting have placed severe restrictions on pharmaceutical development. A number of strategies have been designed to circumvent these limitations, such as liposomes, microspheres, microinjection and adenovirus vectors, but few of these methods have been applied effectively in vivo at a clinical level [1–5]. A group of short polycationic or amphipathic sequences, so-called cell penetrating peptides (CPPs), have attracted much interest, due to their remarkable capacity for passive membrane translocation with low immunogenicity and no toxicity [6,7].

CPPs are a diverse group of 100 or so peptides that are able to cross the cell membrane and deliver various biomolecules into cells; these include oligonucleotides, DNA, siRNA, peptides and proteins as well as liposomes [8–11]. They are regarded as one of the most promising therapeutic tools for non-invasive delivery of macromolecules into cells [12,13], and are therefore likely to play a key role in the future of disease treatments. One of the best-characterized CPPs is derived from the transactivator of transcription (TAT) protein from the human immunodeficiency virus 1 (HIV-1). The minimal peptide sequence of TAT protein responsible for cellular uptake is ^{47}YGRKKRRQRRR^{57} [14], which contains six arginine and two lysine residues and therefore possesses a high net positive charge at physiological pH levels.

Although TAT peptide has been successfully employed for the delivery into cells of a wide variety of compounds [15–20], the exact mechanism of internalization still remains a subject of controversy. Initially, internalization of TAT peptide was understood in terms of cellular endocytosis-mediated uptake, such as clathrin-mediated endocytosis, caveolae-mediated endocytosis, lipid-raft mediated caveolae endocytosis and macropinocytosis [21–25]. In contrast, other reports have favored a direct translocation process that was independent of endocytosis, of temperature, and of a specific receptor, such as transient pore formation, inverted micelles involvement and electroporation-like permeabilization, thereby excluding endocytosis [26–29]. Regardless of the uncertainty of the transmembrane mechanism, it is generally believed that the strong electrostatic attraction between positively-charged TAT peptide and negatively-charged headgroups of phospholipid is a prerequisite for the translocation of peptide [30–34].

* Corresponding author. Tel.: +44 131 650 6139; Fax: +44 131 650 6576.
E-mail address: j.bradshaw@ed.ac.uk (J. Bradshaw).

0005-2736/$ – see front matter © 2013 Elsevier B.V. All rights reserved.
http://dx.doi.org/10.1016/j.bbamem.2013.04.022

A major difficulty in determining the actual mechanism by which TAT peptide acts is that, experimentally, it has proved impossible to observe the insertion of an individual TAT peptide into a plasma membrane in atomic detail. A myriad of indirect physical methods, including fluorescence spectroscopy, differential scanning calorimetry (DSC), isothermal titration calorimetry and nuclear magnetic resonance (NMR), has been employed to localize TAT peptide within model lipid membranes [31–37]. However, they have yielded equivocal and sometimes contradictory results.

With the aim of seeking unambiguous evidence of the location of TAT peptide within lipid bilayers, we employed a direct and sensitive method — neutron lamellar diffraction in combination with H_2O/D_2O substitution. This is the first study we know of in which neutron diffraction was used to observe the interaction of TAT peptide with model phospholipid bilayers. The dioleoylphosphatidylcholine (DOPC) and dioleoylphosphatidylserine (DOPS) were initially considered as model membrane systems because their acyl chains are in the fluid-phase state at the temperature at which our experiments were performed (25 °C), thereby modeling the conditions of a cell membrane under physiological conditions. A mixture of 80:20 mol/mol of DOPC and DOPS phospholipid was used to mimic the negatively-charged state of cell membranes without increasing the complexity of the membrane system unnecessarily. This study gives new insights into the molecular details of the interaction TAT peptide and model anionic model membranes.

2. Materials and methods

2.1. Chemicals

The 11 amino acid TAT peptide (^{47}YGRKKRRQRRR^{57}) was synthesized by Almac Sciences Ltd. (20 Castle Terrace, Edinburgh, EH1 2EN, Scotland, U.K.) using solid-phase synthesis. The purity was >95%, as determined by analytical HPLC, MALDI-TOF mass spectrometry, and amino acid analysis.

1,2-Dioleoyl-sn-glycero-3-phosphocholine (DOPC) and 1,2-dioleoyl-sn-glycero-3-phosphoserine (DOPS) were purchased from Avanti Polar Lipids Inc., USA, and used without further purification. Chloroform, methanol and buffers were all graded AR and purchased from Sigma-Aldrich (Irvine, UK).

2.2. Neutron diffraction

Partially negatively-charged lipid mixture samples were measured on the small momentum transfer diffractometer D16 at the Institut Laue et Langevin (ILL), Grenoble, France. Firstly, TAT peptide was dissolved in Millipore water at 20 mg/mL as a stock solution. Then, 20 mg of an 80:20 (mol%) mixture of DOPC and DOPS were dissolved in chloroform, adding different amounts of TAT peptide stock solution at specific peptide-to-lipid molar ratios (0.1–10 mol%), and finally deposited onto quartz microscope slides (75 mm × 25 mm) by a nitrogen-propelled airbrush. This results in multilayer stacks of highly aligned bilayers. The slides were then placed in a vacuum desiccator for over 12 h in order to remove all traces of the solvent. The samples were protected from light whenever possible in order to reduce the chance of lipid peroxidation. The sample environment was a standard aluminum can, in which temperature control was achieved by circulating water through an integral water jacket and the humidity was controlled by slightly adjusting the temperatures of the solutions in the two Teflon water troughs at the base of the can. Before measurements were made, each sample was hydrated in a backup aluminum can for at least 6 h at a relative humidity of 95%, 97%, and 99%, respectively, and the D_2O concentration was set to 8.06% or 25% (v/v) for each level of relative humidity [38]. Finally, the fully equilibrated sample was quickly transferred straight into the test can and a series of continuous θ–2θ scans were initiated immediately (from θ = 1.5 to 20.0°). All samples were run at 25 °C. Each scan took approximately 3 h to complete and 5 orders of Bragg diffraction were collected. The mosaic spread of the first order of diffraction was determined for each sample using standard procedures. The diffraction intensity was obtained from the detector counts according to the pixel response, and the diffraction images were then collapsed into a linear spectrum for each scan using D16 instrument software LAMP. Background subtraction and peak fitting were performed using PeakFit (SPSS Software). Gaussian distributions were then fitted to the Bragg peaks and the angular position, width and intensity of each peak were recorded. Raw data correction and structure factor amplitude calculations proceeded as previously described [38]. Briefly, the method takes the peak intensities for each order (I_h) and corrects for neutron absorption (C_{abs}) and the Lorentz factor (C_{lor}), resulting in the discrete structure factor amplitudes F(h). Geometry corrections were not needed for the D16 instrument. The two corrections are given by

$$C_{lor} = \sin 2\theta \tag{1}$$

$$C_{abs} = \frac{\alpha}{(1-e^{-\alpha})}, \alpha = \frac{2\mu t}{\sin\theta} \tag{2}$$

where μ is the absorption coefficient, t is the sample thickness, σ is the width of the beam, and μ is the calculated absorption coefficient. The structure factor amplitudes were calculated by taking the square-root of the corrected peak intensities:

$$|F(h)| = \sqrt{C_{abs} C_{abs} I_h}. \tag{3}$$

Above corrected structure factors F(h) were then used for the subsequent Fourier transformation in following section.

2.3. Neutron data analysis

Firstly, the D-repeat (Bragg repeat spacing, d) was calculated by least-squares fitting of the observed angles of diffraction (2θ) to the Bragg equation:

$$n\lambda = 2d \times \sin\theta \tag{4}$$

where n is the order of diffraction, λ is the wavelength of neutrons and θ is the scattering angle.

The structure factors obtained from the same sample at 8.06% D_2O with three different relative humidities can be simultaneously fitted to a single continuous transform in reciprocal space using Shannon's sampling theorem. The procedure was repeated as previously described [39], least-squares fitting the data to sets of model structure factors F(H), each corresponding to a D-repeat of D, and satisfied the following equation:

$$F(h) = \sum_{H=0}^{Hmax} F(H) \frac{\sin\left(\frac{\pi Dh}{d} - \pi H\right)}{\left(\frac{\pi Dh}{d} - \pi H\right)} \tag{5}$$

where F(H) are the sets of model structure factors, F(h) values are the observed structure factors and d is the Bragg repeat spacing.

Finally, phased and scaled structure factors F(h) and Bragg repeat spacings were used to reconstruct coherent relative absolute density profile by Fourier synthesis:

$$\rho(x) = \rho(0) + \frac{2}{d} \sum_{H=0}^{Hmax} F(h) \cos\left(\frac{2\pi x h}{d}\right) \tag{6}$$

where ρ(0) is the average scattering density per unit length of the bilayer, x is the distance along the bilayer normal, F(h) are the scaled structure factors, and the sum describes the distribution in scattering lengths across the bilayer.

As the fact that the bilayer is composed of two monolayers, the average scattering density per unit cell $\rho(0)$ can be estimated by summing the coherent scattering lengths of the atoms that comprise the unit cell.

$$\rho(0) = (2/d)\left(n_w b_w + b_{lip}\right) \quad (7)$$

where n_w is the number of waters per lipid, b_w is the coherent scattering length of water and b_{lip} is the coherent scattering length from a single lipid molecule.

Furthermore, to estimate the significance of any feature in the scattering length density profiles, the errors of the profiles were calculated by [40]

$$\Delta\rho(x) = \frac{2t}{d}\left[\sum_{H=0}^{Hmax} (\Delta F(h))^2 \cos^2\left(\frac{2\pi x h}{d}\right)\right]^{\frac{1}{2}} \quad (8)$$

where $\Delta\rho(x)$ is the error in x at a confidence limit of 95%, t is the Student's t factor (1.96) and $\Delta F(h)$ are the structure factor errors from the fitting process described by Eq. (5).

3. Results and discussion

3.1. D-repeat and bilayer thickness

The isotopic substitution method is the most widely used but time-consuming approach to scale the structure factors from neutron scattering data. In 1998, Bradshaw et al. firstly introduced the swelling-series method that can improve both the accuracy of structure factors measurement and reduce sample equilibration time [38]. The key point of this method is to collect the neutron data at 8.06% D_2O. At this isotopic composition, the negative scattering of hydrogen nuclei is exactly balanced by the positive scattering of oxygen and deuterium nuclei, leading the scattering length density of the water layer is zero [41]. It allows less ambiguous interpretation of the results. Furthermore, the low level of radiation damage of neutrons, due to their non-charged and weak interaction properties, allows several selling-series points can be collected from the same sample. In practice, as the sample was not disturbed between measurements, the requirement for scaling between measurements in the same swelling series was not needed. Another advantage of the swelling-series method was that any bilayer disturbance and modification induced by peptide or protein would have a direct reflection in the lipid scattering length density (SLD) profile, due to the strong positive scattering length from their chemical compositions like carbon, nitrogen, and oxygen. It was straightforward to locate the peptide distribution through the bilayer by comparing the lipid SLD profiles in the presence and absence of peptide.

All the experimentally derived structure factors used to calculate transbilayer SLD profiles in the presence of 8.06 mol% D_2O, including the form factor errors from the fitting procedure as described in Methods, are summarized in Table 1.

From Table 2, the D-repeat of DOPC/DOPS (80:20) mixture bilayer, calculated using the Bragg equation from 5 orders of diffraction at a relative humidity of 99%, was 52.55 ± 0.40 Å (mean ± SD, n = 5). Interestingly, when up to 1 mol% peptide (peptide/lipid ratio) was introduced, no significant difference in D-repeat was found. The D-repeats of various samples were 52.62 ± 0.41 Å and 52.53 ± 0.37 Å, for DOPC/DOPS with 0.1 mol% TAT and 1 mol% TAT, respectively. These differences in D-repeat were well within the generally accepted error limit (up to 1 Å) [42]. However, a significant 2 Å increase in D-repeat was observed at 10 mol% peptide concentration, compared to the pure lipid (54.62 ± 0.40 Å vs. 52.55 ± 0.40 Å).

Table 2
d-repeat and bilayer thickness of DOPC/DOPS bilayer in presence and absence of TAT peptide at 99%RH, with 8% ^2H_2O.

P/L ratio	0%	0.1%	1%	10%
d-repeat (Å)	52.55 ± 0.40	52.62 ± 0.41	52.53 ± 0.37	54.62 ± 0.40
Bilayer thickness (Å)	34.97 ± 0.30	34.97 ± 0.30	33.94 ± 0.26	33.94 ± 0.26

We also extracted the bilayer thickness information from the scattering length density (SLD) profile of lipid bilayer at 8.06% D_2O, as shown in Fig. 1, which, for this purpose, may be defined as the distance between the two maxima in the profile. The two maxima in a typical bilayer profile corresponded to the glycerol backbone and phosphate headgroups. The oxygens of the ester linkages attaching the fatty-acyl chains and head group to the glycerol, and the phosphorus and oxygen atoms of the headgroups increased the scattering length density of this region. Values for the bilayer hydrophobic thickness are presented in Table 1. When a small amount of TAT peptide was firstly introduced, no difference in bilayer thickness was found. Membrane thinning only occurred when the peptide concentration reached a threshold (1 mol%). The bilayer thickness shrank from 34.97 ± 0.30 Å for the 0.5 mol% sample to 33.94 ± 0.26 Å for the 1 mol% sample, and remained constant when more peptides were incorporated. The amount of thinning was not directly proportional to the peptide concentration.

Taken together, the above data from D-repeat and bilayer thickness showed that TAT peptide did lead to thinning of anionic membranes, above a certain concentration threshold (1 mol%). Moreover, the largest TAT peptide concentration investigated (10 mol%) might be larger than the saturation of the insertion, thus a significant amount of peptide remained in the aqueous bulk between adjacent bilayers. This would explain why a 2 Å increase in D-repeat was observed at 10 mol% peptide concentration, whereas the bilayer thickness remained unchanged.

3.2. Scattering length density profiles

As described above, under the conditions of 8.06% D_2O, neutron scattering by the water was eliminated and the water was effectively invisible to neutrons; the resulting SLD profile came from the diffraction of the lipid only [38]. Fig. 1 shows the SLD profiles of pure DOPC/DOPS bilayers (black solid line) and of DOPC/DOPS with different amount of TAT peptide (black broken line) at 8.06% D_2O. Typical structure features of the lamellar lipid bilayer were well represented in the pure lipid SLD profile. [43]. The origin of the x-axis was the centrosymmetric center of the unit cell, which corresponded to the center of the bilayer. The interlamellar water layers lay at the two edges of the unit cell. Two maxima in the profile corresponded to the polar lipid headgroups, which were a combination of glycerol-ester and phosphate moieties. A minimum at the center of the profile corresponded to the terminal methyl

Table 1
Experimental determined, corrected, and scaled structure factors of DOPC/DOPS mixture lipid bilayers (8:2) in absence and presence of different concentrations of TAT peptide.

P/L ratio	F(1)	F(2)	F(3)	F(4)	F(5)
0%	−21.21 ± 0.50	−11.29 ± 0.02	8.94 ± 0.03	−5.44 ± 0.01	−2.68 ± 0.11
0.1%	−26.32 ± 0.78	−13.56 ± 0.10	10.74 ± 0.13	−6.39 ± 0.21	−3.73 ± 0.01
1%	−32.68 ± 0.01	−16.06 ± 0.34	12.17 ± 0.07	−5.99 ± 0.01	−4.35 ± 0.13
10%	−48.56 ± 0.68	−18.75 ± 0.50	10.86 ± 0.01	−2.84 ± 0.22	−5.68 ± 0.10

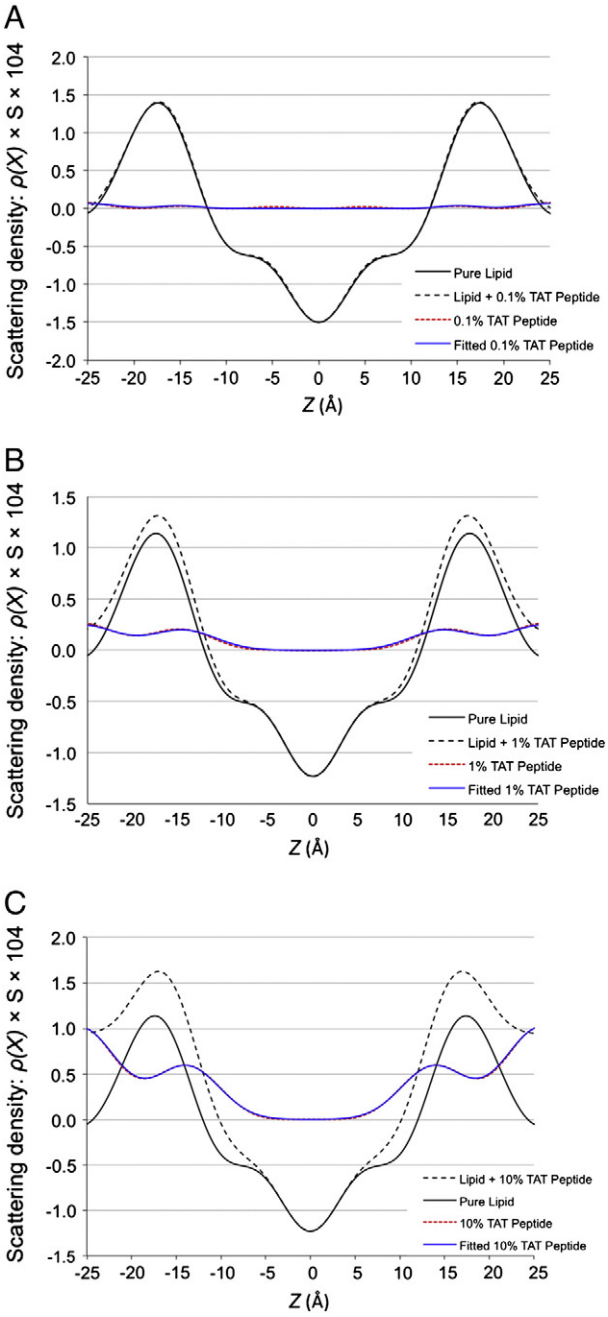

Fig. 1. An illustration of neutron scattering length density (SLD) profiles at 8.06% ^2H_2O. Pure DOPC/DOPS lipid bilayer is drawn in black solid line and of lipid with 1 mol% TAT peptide is drawn in black broken line. The difference profile calculated by subtracting structure factors of pure lipid from structure factors of lipid with TAT peptide is shown in red broken line. A fit of two Gaussian functions to the difference profile is shown in blue solid line. From A to C, the amount of TAT peptide is increased.

groups of the lipids. The two small kinks between maximum and minimum represented the double bond in oleoyl fatty acid chains. From the above detailed depiction of lipid SLD profile, it was convenient to use the distance between these two maxima as an indication of bilayer thickness, though it more precisely represented the thickness of the bilayer between the glycerol backbones, and did not take into account much of the bilayer headgroup above the phosphate [44].

A series of experiments had been conducted to compare the peptide distribution at different peptide concentrations (0.1 mol% to 10 mol%) in the DOPC/DOPS mixture lipid bilayer. Appropriate raw neutron diffraction data were phased and placed on a relative absolute scale to reconstruct the SLD profiles by Fourier synthesis. In Fig. 1, the red broken line is the difference between two lipid SLD profiles under 8.06% D_2O in the presence and absence of peptide, representing the transbilayer peptide distribution. The difference profile could be fitted as two Gaussian-shaped peaks in reciprocal space following the procedure already described [38–40]. By comparing the calculated structure factors of each difference SLD profile to the observed difference structure factors, two resulting parameters from the Gaussian fitting revealed important information of transbilayer peptide distribution. The first parameter was the position of the peak, which was located at the time-averaged center-of-mass (strictly, the center of SLD) of TAT peptide, as measured from the center of the bilayer. The second parameter was the width of the peak, which indicated the time-averaged fluctuation amplitude of TAT peptides across the lipid bilayer. As shown in Fig. 1, the blue solid line was a fit of a single Gaussian function to the difference profile, and whose parameters are summarized in Table 3. It should be pointed that all comparisons of the calculated and observed SLD profiles were carried out in real space, and the Gaussian fitting was carried out in reciprocal space.

From Fig. 1A, no significant difference in the SLD profiles in the presence and absence of 0.1 mol% TAT peptide were detected. However, these two SLD profiles did not overlap perfectly. Indeed, two small increases of SLD density were located around the two edges of the unit cell and the polar lipid headgroups of lipid, which were the same positions found when higher peptide concentrations were investigated. The neutron scattering length density of the peptide is similar to that of the phospholipids, so it is not surprising that the changes in SLD profile are so small. However, when considered in combination with other factors, as described below, we preferred to interpret this observation not as an experimental error but as an important clue that the intercalation of TAT peptides inside the glycerol region of lipid and the perturbations of a lipid bilayer by TAT peptides happened even at very low peptide content (0.1%).

3.3. Peptide distribution in DOPC/DOPS lipid bilayer

From Fig. 2, and Table 3, the best fits to observed peptide profiles clearly demonstrated that the interaction of TAT peptide with negatively-charged DOPC/DOPS lipid bilayer took place at two positions. A part of peptides was intercalated into the lipid/water interface region of the bilayer at around 14.3 Å from the center of the lipid bilayer. The rest of peptides located in the peripheral aqueous phase between adjacent bilayers at around 24.6 Å from the center of the lipid bilayer. With increasing peptide concentration, the first peptide distribution at lipid/water interface region started to shift toward to the center of the lipid bilayer, whereas the second distribution at aqueous phase did not move. The center mass of the peptide was found to reside 15.2 Å from the center of the bilayer at 0.1 mol% peptide concentration, while the corresponding value for 1 mol% peptide concentration was 14.3 Å, moving 0.9 Å closer to the center of the bilayer. In the DOPC/DOPS mixture lipid, this location was very close to the glycerol backbone region. Taking into account the observation that the bilayer thickness of high peptide concentration sample was 1 Å thinner than that of

Table 3
Summary of parameters of the Gaussian fits of the calculated peptide (difference SLD) profiles in reciprocal space. Five orders of diffraction were used in the fitting procedure. The position of TAT peptide is expressed as the distance from the center of the bilayer. The width is the full width at half height.

TAT peptide distribution		L/P = 100:0.1	L/P = 100:1	L/P = 100:10
Gaussian 1	Position (Å)	23.7	24.8	24.6
	Width (Å)	3.3	5.6	5.5
	Occupancy (%)	57.9	41.5	49.3
Gaussian 2	Position (Å)	15.2	14.3	13.8
	Width (Å)	3.0	5.1	5.1
	Occupancy (%)	42.1	58.5	50.7

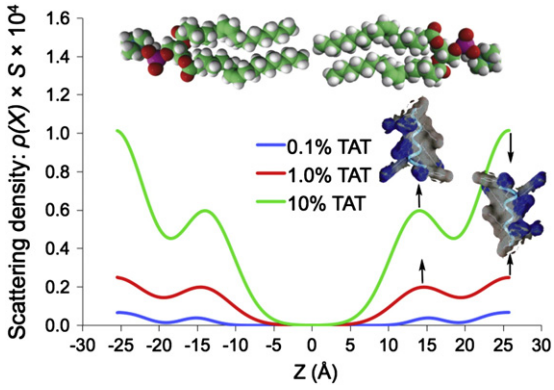

Fig. 2. Summary of Gaussian fitting results to observed peptide (difference SLD) profiles at a series of peptide concentrations, representing two TAT peptide distributions in negatively-charged DOPC/DOPS bilayers. The interbilayer water compartment is at the two edges of the graph. A pair of phospholipid molecules is shown above the graph to illustrate the orientation of the lipid bilayer. The comparison is set on the same d-repeat. From the bottom to the top, the amount of TAT peptide is increased. The molecular structures of TAT peptide are derived from Ho et al. [45]. The hydrophilic surface region of peptide is colored in blue, and the hydrophobic surface region is colored in gray.

low concentration sample (33.9 Å vs. 34.9 Å), we suggested that TAT peptide was at nearly the same location relative to the lipid molecule.

In addition, the width of peptide distribution showed little change after addition of the peptide to the bilayer. Even increasing the amount of peptide to the largest concentration (10 mol%) made little difference to the width of peptide distribution obtained, which meant that TAT peptide was motionally constrained to an around 5 Å region at the lipid/water interface. Moreover, Gaussian fitting to the difference SLD profiles also yielded the amount of TAT peptide located in the bilayer. Interestingly, even at the lowest peptide concentration investigated (0.1 mol%), 42% of peptides were positioned below the glycerol backbone region of the bilayer and 58% remained in the aqueous phase between adjacent bilayers. Such proportions of TAT peptide distribution in the bilayer did not significantly change over the entire range of peptide concentrations investigated. This indicated that the peptide has two preferred locations relative to the bilayer. It was likely that the distribution of individual peptide molecules between the two locations was a dynamic, rather than static, equilibrium. Unfortunately the time scale of our neutron measurements did not allow this to be determined. The bilayer profiles represented time-averaged distributions of neutron scattering length. The preference for the surface location (58% of the peptide) was probably due to the electrostatic attraction between the negatively-charged headgroup of phospholipid and positively charged TAT peptide.

However, the above results also strongly indicated an intrinsic affinity between TAT peptide and a location just below the glycerol backbone region of the phospholipid bilayer. This was completely in agreement with recent work reported by Su et al. [46], who proposed that TAT peptides penetrated the glycerol backbone region of the DMPC/DMPG bilayers and occupied a 5.5 Å region at the lipid/water interface using Solid-State NMR.

Our findings, furthermore, raised an intriguing question as to why TAT peptide remained at the same penetration depth and width in the DOPC/DOPS lipid bilayer. Recently, an interesting study on CPPs and antimicrobial peptides has suggested that the structural basis for the rapid translocation of arginine-rich CPPs may lie in the ability of guanidinium to form hydrogen-bond stabilized bidentate complexes with lipid phosphates, which cannot be achieved by the mobile amine of the Lys side chains [46]. Based on this assumption, we prefer to think that guanidinium-phosphate ion pair interaction between the arginine residues and phosphate groups of phospholipids, rather that the electrostatic attraction between the peptide and negative-charged headgroups, might be the determining factor for the membrane translocation of TAT peptide. This would be a reasonable explanation as to why TAT preferred to locate the inner glycerol region of phospholipid, while facing un-neglected anionic membrane backgroups. To investigate this hypothesis, further neutron diffractions experiments focusing on the interaction between TAT peptide and neutral zwitterionic phospholipids like DOPC are in progress.

3.4. Water distribution in DOPC/DOPS lipid bilayer

Additional support for the penetration of the peptide into the lipid bilayer was given by the water distribution across the lipid bilayer. The dependence of the SLD profile on the D_2O content in water vapor enabled the calculation of the water distribution across the bilayer by subtracting the structure factors 8.06% D_2O from those at high D_2O concentration (25%). All fitted water profiles are presented in Fig. 3 for easy comparison and the resultant parameters from the Gaussian fitting are summarized in Table 4. A typical distribution of water in the pure lipid bilayer was fitted well by a single Gaussian peak at the two edges of the crystallographic unit cell, representing the water layer between adjacent bilayers [38]. The corresponding water distribution profiles lipid samples containing different TAT peptide concentrations were very similar, and were centered around 22.5 Å from the center of the bilayer and on 6.5 Å wide. The water distribution profiles in Fig. 3 show increasing amounts of water as the amount of peptide increases. This probably represented the additional water required to hydrate the peptide, plus hydrogen-deuterium exchange on the peptide. Furthermore, the water density in the lipid hydrophobic core was marginal, indicating that no water penetrated into this region at a peptide concentration lower than 10 mol%. However, for the lipid sample with 10 mol% TAT peptide, 16% of water population deeply intercalated inside the hydrophobic core at 6.2 Å from the center of the bilayer, a position close to the double bonds of the oleoyl acyl chain. Meanwhile, the width of this water distribution was 3.6 Å, covering almost of whole hydrophobic region of the bilayer, which was direct evidence for the formation of a transbilayer water channel.

Taking the above information together, the bilayer thinning, the motional constraint of the peptide below the glycerol backbone region, the discrete peptide distribution across the bilayer, and the presence of a contiguous transbilayer water channel at a threshold concentration, the neutron scattering data presented here unambiguously support the carpet model of membrane perturbation induced by TAT peptide. However, based on the well-studied pore formation models of antimicrobial peptides, peptide surface carpeting and bilayer thinning are very early characteristics of peptide–membrane interactions, which may subsequently lead to conditions allowing a local membrane

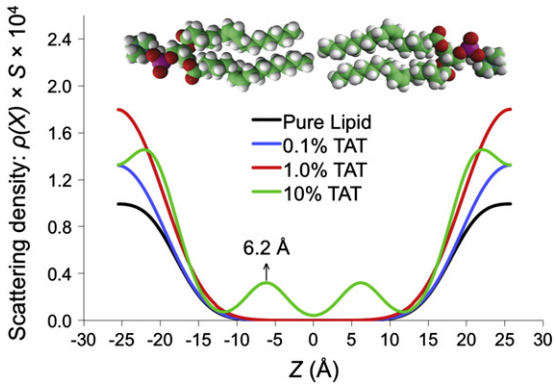

Fig. 3. Summary of Gaussian fitting results to observed water (difference SLD) profiles at a series of TAT peptide concentrations in negatively-charged DOPC/DOPS lipid bilayers. The interbilayer water compartment is at the two edges of the graph. A pair of phospholipid molecules is shown above the graph to illustrate the orientation of the lipid bilayer. The comparison is set on the same d-repeat.

Table 4
Summary of parameters of the Gaussian fits of the calculated water profiles in reciprocal space. Five orders of diffraction were used in the fitting procedure. The position of water is expressed as the distance from the center of the bilayer. The width is the full width at half height.

Water distribution		Pure lipid	L/P = 100:0.1	L/P = 100:1	L/P = 100:10
Gaussian 1	Position (Å)	21.8	22.5	22.7	21.4
	Width (Å)	5.9	6.4	6.8	5.1
	Occupancy (%)	100	100	100	85.2
Gaussian 2	Position (Å)	–	–	–	6.2
	Width (Å)	–	–	–	3.6
	Occupancy (%)	–	–	–	15.8

perturbation to form a lipid–peptide toroidal pore structure or a detergent-like disintegration of the bilayer structure [47–51].

The detergent-like model was ruled out, because in this model the membrane would be permeated and disintegrated in a detergent like manner without the formation of intermediate discrete water channels [48–52]. Back to our neutron data, despite a contiguous transbilayer water channel was observed, at least up to 5 orders of diffraction signal were detected in the largest peptide concentration investigated (10 mol%) (Data not shown here), strongly indicating that the bilayer at this experimental condition remained highly lamellar in structure.

The peptide barrel-stave model was also excluded for the following reason. Amphipathic α-helical peptides insert in a perpendicular orientation to the plane of the bilayer, with the hydrophobic sides of helices facing fatty acid chains and hydrophilic sides self-assembling a pore, without peptide surface carpet conformation [53–55]. However, from our CD data (data not shown here), TAT peptide mainly adopted a random-coil structure upon interaction with the same model DOPC/DOPS membrane (80:20) employed in this neutron diffraction experiment. More importantly, the structure of the barrel-stave model addressed the fact that TAT peptide was simply too short to span an undisturbed lipid bilayer without thinning. A typical width 32–38 Å of bilayer was clearly far beyond the limit of an 11-amino acid TAT peptide [56,57].

Thus, the toroidal pore model was strongly suggested, as the data observed in this paper were mostly in agreement with all the detailed aspects of the toroidal pore model. For example, a limited number of peptides first assembled on the lipid bilayer surface and then inserted into the bilayer with the hydrophilic regions of the peptides associating with the phospholipid headgroups while the hydrophobic regions associated with the lipid core [49–51]. As soon as a threshold concentration of peptide was reached, a significant rearrangement of lipid bilayer happened and transient pores could be formed.

However, it should be noted that the amount of bilayer thinning described in our paper was not directly proportional to the peptide concentration, which was an obvious difference between the theoretical model and the experimental data. Moreover, it was also somewhat questionable that whether the toroidal pore model was the actual transmembrane mechanism of TAT peptide, as the contiguous transbilayer water channel and the toroidal pore formation occurred at an unphysiologically high threshold concentration of TAT peptide in our experiments. Most importantly, in contrast to those arginine-rich antimicrobial peptides (AMPs) which kill bacterial cells by pore formation mechanism, TAT peptide appears to translocate into eukaryotic cells without causing long-lasting damage to the integrity of the cell membrane and at very low peptide concentrations [37,58]. The elucidation of the exact mechanism involved in the transmembrane of TAT peptide is complicated by these apparent discrepancies, however, we are confident that their presence does not detract from the valuable structural information, revealed here by the use of neutron lamellar diffraction, that TAT peptide carpets the glycerol backbone region of the bilayer.

4. Conclusion

In conclusion, our data presented the first study of the interaction between TAT peptide and negatively-charged DOPC/DOPS mixture lipid bilayer, using neutron lamellar diffraction. The results unambiguously showed that the interaction of TAT peptide with anionic lipid bilayers took place at two locations. One was in the peripheral aqueous phase between the adjacent bilayers and the second one was below the glycerol backbone region of the lipid bilayer. In addition, we found that TAT peptide carpeted the glycerol backbone region of the lipid bilayer over all the peptide concentrations investigated. A concentration-independent membrane thinning above a peptide concentration threshold (1 mol%) and a contiguous transbilayer water channel at the largest peptide concentration (10 mol%) were also found. This evidence led to the suggestion that the toroidal pore model might be involved in the transmembrane mechanism of TAT peptide. Moreover, we interpreted the surface peptide distribution in the peripheral aqueous phase as a massive exclusion of TAT peptide from its intrinsic location below the glycerol backbone region of the bilayer. This was due to the electrostatic attractions between the negatively-charged headgroups of phospholipid and the positively charged TAT peptides. It consequently further led to the argument that the role negative-charged headgroups of DOPS lipid play in the transmembrane of TAT peptide is less important than previously thought. To test this hypothesis, further neutron diffractions experiments focusing on the interaction between TAT peptide and neutral zwitterionic phospholipids like DOPC will be conducted in the future. And more precise investigations using a TAT peptide with the deuterated fragment on the C-terminal and N-terminal side will also be carried out. The localization of these labels will provide the exact orientation information of TAT peptide inside the bilayers. It is hoped that our data presented here will stimulate further structure studies on the transmembrane of TAT peptide, like molecular dynamics simulations.

Acknowledgement

This work is supported by an Overseas Research Scholarship from The University of Edinburgh and the Institute Laue-Langevin.

References

[1] R.M. Mainardes, L.P. Silva, Drug delivery systems: past, present, and future, Curr. Drug Targets 5 (2004) 449–455.
[2] K. Lundstrom, T. Boulikas, Viral and non-viral vectors in gene therapy: technology development and clinical trials, Technol. Cancer Res. Treat. 2 (2003) 471–486.
[3] J.W. Schott, M. Galla, T. Godinho, C. Baum, A. Schambach, Viral and non-viral approaches for transient delivery of mRNA and proteins, Curr. Gene Ther. 11 (2011) 382–398.
[4] S. Mehier-Humbert, R.H. Guy, Physical methods for gene transfer: improving the kinetics of gene delivery into cells, Adv. Drug Deliv. Rev. 57 (2005) 733–753.
[5] A. El-Aneed, An overview of current delivery systems in cancer gene therapy, J. Control. Release 94 (2004) 1–14.
[6] A. Prochiantz, Protein and peptide transduction, twenty years later a happy birthday, Adv. Drug Deliv. Rev. 60 (2008) 448–451.
[7] S.B. Fonseca, M.P. Pereira, S.O. Kelley, Recent advances in the use of cell-penetrating peptides for medical and biological applications, Adv. Drug Deliv. Rev. 61 (2009) 953–964.
[8] B. Gupta, T.S. Levchenko, V.P. Torchilin, Intracellular delivery of large molecules and small particles by cell-penetrating proteins and peptides, Adv. Drug Deliv. Rev. 57 (2005) 637–651.
[9] E. Vivès, J. Schmidt, A. Pèlegrin, Cell-penetrating and cell-targeting peptides in drug delivery, Biochim. Biophys. Acta 1786 (2008) 126–138.
[10] M. Law, M. Jafari, P. Chen, Physicochemical characterization of siRNA-peptide complexes, Biotechnol. Prog. 24 (2008) 957–963.
[11] N.A. Brooks, D.S. Pouniotis, C.K. Tang, V. Apostolopoulos, G.A. Pietersz, Cell-penetrating peptides: application in vaccine delivery, Biochim. Biophys. Acta 1805 (2010) 25–34.
[12] F. Heitz, M.C. Morris, G. Divita, Twenty years of cell-penetrating peptides: from molecular mechanisms to therapeutics, Br. J. Pharmacol. 157 (2009) 195–206.
[13] M.C. Morris, S. Deshayes, F. Heitz, G. Divita, Cell-penetrating peptides: from molecular mechanisms to therapeutics, Biol. Cell. 100 (2008) 201–217.

[14] E. Vivès, P. Brodin, B. Lebleu, A truncated HIV-1 Tat protein basic domain rapidly translocates through the plasma membrane and accumulates in the cell nucleus, J. Biol. Chem. 272 (1997) 16010–16017.
[15] H. Brooks, B. Lebleu, E. Vivès, Tat peptide-mediated cellular delivery: back to basics, Adv. Drug Deliv. Rev. 57 (2005) 559–577.
[16] J.S. Wadia, S.F. Dowdy, Transmembrane delivery of protein and peptide drugs by TAT-mediated transduction in the treatment of cancer, Adv. Drug Deliv. Rev. 57 (2005) 579–596.
[17] I.N. Shokolenko, M.F. Alexeyev, S.P. LeDoux, G.L. Wilson, TAT-mediated protein transduction and targeted delivery of fusion proteins into mitochondria of breast cancer cells, DNA Repair (Amst) 4 (2005) 511–518.
[18] J.L. Johnson, B.C. Lowell, O.P. Ryabinina, R.S. Lloyd, A.K. McCullough AK, TAT-mediated delivery of a DNA repair enzyme to skin cells rapidly initiates repair of UV-induced DNA damage, J. Invest. Dermatol. 131 (2011) 753–761.
[19] I.A. Ignatovich, F.B. Dizhe, A.V. Pavlotskaya, B.N. Akifiev, S.V. Burov, S.V. Orlov, A.P. Perevozchikov, Complexes of plasmid DNA with basic domain 47–57 of the HIV-1 Tat protein are transferred to mammalian cells by endocytosis-mediated pathways, J. Biol. Chem. 278 (2003) 42625–42636.
[20] J.A. MacKay JA, W. Li, Z. Huang, E.E. Dy, G. Huynh, T. Tihan, R. Collins, D.F. Deen, F.C. Szoka Jr., HIV TAT peptide modifies the distribution of DNA nanolipoparticles following convection-enhanced delivery, Mol. Ther. 16 (2008) 893–900.
[21] I. Nakase, M. Niwa, T. Takeuchi, K. Sonomura, N. Kawabata, Y. Koike, M. Takehashi, S. Tanaka, K. Ueda, J.C. Simpson, A.T. Jones, Y. Sugiura, S. Futaki, Cellular uptake of arginine-rich peptides: roles for macropinocytosis and actin rearrangement, Mol. Ther. 10 (2004) 1011–1022.
[22] J.S. Wadia, R.V. Stan, S.F. Dowdy, Transducible TAT-HA fusogenic peptide enhances escape of TAT-fusion proteins after lipid raft macropinocytosis, Natl. Med. 10 (2004) 310–315.
[23] J.P. Richard, K. Melikov, H. Brooks, P. Prevot, B. Lebleu, L.V. Chernomordik, Cellular uptake of unconjugated TAT peptide involves clathrin-dependent endocytosis and heparan sulfate receptors, J. Biol. Chem. 280 (2005) 15300–15306.
[24] I. Nakase, A. Tadokoro, N. Kawabata, T. Takeuchi, H. Katoh, K. Hiramoto, M. Negishi, M. Nomizu, Y. Sugiura, S. Futaki, Interaction of arginine-rich peptides with membrane-associated proteoglycans is crucial for induction of actin organization and macropinocytosis, Biochemistry 46 (2007) 492–501.
[25] A. Fittipaldi, A. Ferrari, M. Zoppé, C. Arcangeli, V. Pellegrini, F. Beltram, M. Giacca, Cell membrane lipid rafts mediate caveolar endocytosis of HIV-1 Tat fusion proteins, J. Biol. Chem. 278 (2003) 34141–34149.
[26] D. Terrone, S.L. Sang, L. Roudaia, J.R. Silvius, Penetratin and related cell-penetrating cationic peptides can translocate across lipid bilayers in the presence of a transbilayer potential, Biochemistry 42 (2003) 13787–13799.
[27] J.B. Rothbard, T.C. Jessop, R.S. Lewis, B.A. Murray, P.A. Wender, Role of membrane potential and hydrogen bonding in the mechanism of translocation of guanidinium-rich peptides into cells, J. Am. Chem. Soc. 126 (2004) 9506–9507.
[28] P.E. Thorén, D. Persson, P. Isakson, M. Goksör, A. Onfelt, B. Nordén, Uptake of analogs of penetratin, Tat(48–60) and oligoarginine in live cells, Biochem. Biophys. Res. Commun. 307 (2003) 100–107.
[29] H. Binder, G. Lindblom, Charge-dependent translocation of the Trojan peptide penetratin across lipid membranes, Biophys. J. 85 (2003) 982–995.
[30] V.P. Torchilin, Tat peptide-mediated intracellular delivery of pharmaceutical nanocarriers, Adv. Drug Deliv. Rev. 60 (2008) 548–558.
[31] V. Tiriveedhi, P. Butko, A fluorescence spectroscopy study on the interactions of the TAT-PTD peptide with model lipid membranes, Biochemistry 46 (2007) 3888–3895.
[32] A. Ziegler A, X.L. Blatter, A. Seelig, J. Seelig, Protein transduction domains of HIV-1 and SIV TAT interact with charged lipid vesicles. Binding mechanism and thermodynamic analysis, Biochemistry 42 (2003) 9185–9194.
[33] M. Lundberg, S. Wikstrom, M. Johansson, Cell surface adherence and endocytosis of protein transduction domains, Mol. Ther. 8 (2003) 143–150.
[34] E. Vives, J.P. Richard, C. Rispal, B. Lebleu, TAT peptide internalization: seeking the mechanism of entry, Curr. Protein Pept. Sci. 4 (2003) 125–132.
[35] S. Hakansson, M. Caffrey, Structural and dynamic properties of the HIV-1 tat transduction domain in the free and heparin-bound states, Biochemistry 42 (2003) 8999–9006.
[36] S. Afonin, A. Frey, S. Bayerl, D. Fischer, P. Wadhwani, S. Weinkauf, A.S. Ulrich, The cell-penetrating peptide TAT(48–60) induces a non-lamellar phase in DMPC membranes, ChemPhysChem 7 (2006) 2134–2142.
[37] I.D. Alves ID, I. Correia, C.Y. Jiao, E. Sachon, S. Sagan, S. Lavielle, G. Tollin, G. Chassaing, The interaction of cell-penetrating peptides with lipid model systems and subsequent lipid reorganization: thermodynamic and structural characterization, J. Pept. Sci. 15 (2009) 200–209.
[38] J.P. Bradshaw, M.J.M. Darkesa, S.M.A. Davies, Improved accuracy and phasing of lamellar neutron diffraction data by real-time swelling series method, Physica B 241–243 (1998) 1115–1121.
[39] C.R. Worthington, G.I. King, Electron density profiles of nerve myelin, Nature 234 (1971) 143–145.
[40] R.H. Ashley RH, T.A. Harroun, T. Hauss, K.C. Breen, J.P. Bradshaw, Autoinsertion of soluble oligomers of Alzheimer's Abeta (1–42) peptide into cholesterol-containing membranes is accompanied by relocation of the sterol towards the bilayer surface, BMC Struct. Biol. 19 (2006) 21.
[41] M.J. Darkes, J.P. Bradshaw, Real-time swelling-series method improves the accuracy of lamellar neutron-diffraction data, Acta Crystallogr. D: Biol. Crystallogr. 56 (2000) 48–54.
[42] T. Hauss, S. Dante, T.H. Haines, N.A. Dencher, Localization of coenzyme Q10 in the center of a deuterated lipid membrane by neutron diffraction, Biochim. Biophys. Acta 1710 (2005) 57–62.
[43] D.L. Worcester DL, N.P. Franks, Structural analysis of hydrated egg lecithin and cholesterol bilayers. II. Neutrol diffraction, J. Mol. Biol. 100 (1976) 359–378.
[44] G.I. King, S.H. White, Determining bilayer hydrocarbon thickness from neutron diffraction measurements using strip-function models, Biophys. J. 49 (1986) 1047–1054.
[45] A. Ho, S.R. Schwarze, S.J. Mermelstein, G. Waksman, S.F. Dowdy, Synthetic protein transduction domains: enhanced transduction potential in vitro and in vivo, Cancer Res. 61 (2001) 474–477.
[46] Y. Su, A.J. Waring, P. Ruchala, M. Hong, Membrane-bound dynamic structure of an arginine-rich cell-penetrating peptide, the protein transduction domain of HIV TAT, from solid-state NMR, Biochemistry 49 (2010) 6009–6020.
[47] E. Gazit, I.R. Miller, P.C. Biggin, M.S. Sansom, Y. Shai, Structure and orientation of the mammalian antibacterial peptide cecropin P1 within phospholipid membranes, J. Mol. Biol. 258 (1996) 860–870.
[48] Y. Shai, Mode of action of membrane active antimicrobial peptides, Biopolymers 66 (2002) 236–248.
[49] H.W. Huang, Action of antimicrobial peptides: two-state model, Biochemistry 39 (2000) 8347–8352.
[50] L. Yang, T.A. Harroun, T.M. Weiss, L. Ding, H.W. Huang, Barrel-stave model or toroidal model? A case study on melittin pores, Biophys. J. 81 (2001) 1475–1485.
[51] S.J. Ludtke, K. He, W.T. Heller, T.A. Harroun, L. Yang, H.W. Huang, Membrane pores induced by magainin, Biochemistry 35 (1996) 13723–13728.
[52] E. Gazit, A. Boman, H.G. Boman, Y. Shai, Interaction of the mammalian antibacterial peptide cecropin P1 with phospholipid vesicles, Biochemistry 34 (1995) 11479–11488.
[53] P. Mueller, D.O. Rudin, Action potentials induced in biomolecular lipid membranes, Nature 217 (1968) 713–719.
[54] D.S. Cafiso, Alamethicin: a peptide model for voltage gating and protein–membrane interactions, Annu. Rev. Biophys. 23 (1994) 141–165.
[55] M. Barranger-Mathys, D.S. Cafiso, Collisions between helical peptides in membranes monitored using electron paramagnetic resonance: evidence that alamethicin is monomeric in the absence of a membrane potential, Biophys. J. 67 (1994) 172–176.
[56] K. He, S.J. Ludtke, D.L. Worcester, H.W. Huang, Neutron scattering in the plane of membranes: structure of alamethicin pores, Biophys. J. 70 (1996) 2659–2666.
[57] Y.P. Zhang, R.N. Lewis, R.S. Hodges, R.N. McElhaney, Peptide models of helical hydrophobic transmembrane segments of membrane proteins: II. Differential scanning calorimetric and FTIR spectroscopic studies of the interaction of Ac-K2-(LA)12-K2-amide with phosphatidylcholine bilayers, Biochemistry 34 (1995) 2362–2371.
[58] V.P. Torchilin, R. Rammohan, V. Weissig, T.S. Levchenko, TAT peptide on the surface of liposomes affords their efficient intracellular delivery even at low temperature and in the presence of metabolic inhibitors, Proc. Natl. Acad Sci. U. S. A. 98 (2001) 8786–8791.